
Climate Change Initiative Extension (CCI+) Phase 2
New Essential Climate Variables (NEW ECVS)
High Resolution Land Cover ECV (HR_LandCover_cci)

Climate Assessment Report
(CAR)

Prepared by:

Università degli Studi di Trento
Fondazione Bruno Kessler
Università degli Studi di Pavia
Università degli Studi di Genova
Université Catholique de Louvain
Politecnico di Milano
LSCE
CREAF
University of Exeter
e-GEOS s.p.a.
Planetek Italia





UNIVERSITY
OF TRENTO



UCLouvain
Earth and Life Institute - Geomatics



	Ref	D5.1 - CAR		
	Issue	Date	Page	
	1.0	20/12/2024	1	

Changelog



Issue	Changes	Date
1.0	First issue	20/12/2024

Detailed Change Record

Issue	RID	Description of discrepancy	Sections	Change

Contents

1	Introduction.....	2
1.1	Executive summary	2
1.2	Purpose and scope	2
1.3	Applicable documents.....	3
1.4	Reference documents	3
1.5	Acronyms and abbreviations.....	3
2	Role of spatial resolution and vegetation type uncertainties on the simulation of biogeochemical fluxes ..	3
2.1	Role of spatial resolution on ORCHIDEE simulated biogeochemical fluxes	4
2.2	Methodology.....	4
2.3	Generation of fraction LC maps at 0.1° from 10m and 30m HRLC maps	5
2.4	Comparison between 10m and 30m maps	6
2.5	Impacts on ORCHIDEE energy, water and carbon fluxes	10
3	Drought climate service	15
3.1	Climate data	15
3.2	Look up table linking land cover types and drought models	16
3.3	Integration approach	17

	Ref	D5.1 - CAR		
	Issue	Date	Page	
	1.0	20/12/2024	2	

1 Introduction

1.1 Executive summary

The Climate Assessment Report offers detailed insights into the practical applications and user feedback concerning the Climate Research Data Package (CRDP) version 1. This package, which can be accessed at [CEDA's online catalogue](#), has been evaluated for its utility, relevance, and significance in supporting climate research and decision-making. The report captures a comprehensive assessment from the climate research community, highlighting both the strengths of CRDP v1 and areas where further refinement is required. The assessment is based on the 3 case studies included in Task 5 of the project aiming to carry out all climatological assessments to establish the value of the products and finally set up a complete Climate Research Data Package open to the community with the stated requirements:

1. The role of spatial resolution and vegetation on the simulation of biogeochemical fluxes (LSCE supported by CREAM)
2. The use of HRLC products for improving drought climate data monitoring (CREAF)
3. Deriving deforestation maps of Amazonia from HRLC products to improve Global Carbon Budget assessments (UNEXE)

The findings presented in this document serve as a critical resource for guiding future enhancements to the CRDP, ensuring that subsequent iterations are more robust, user-friendly, and aligned with the evolving needs of the climate science community. Feedback from this assessment will directly inform the development of improved datasets and tools, fostering more effective climate modelling and analysis.

In summary, this first version of the CAR document presents the following designed methodologies and results:



- the methodology followed to generate ORCHIDEE PFT maps at various scales
- the results of the ORCHIDEE simulations on the 3 regions and for the 10m and 30m derived PFT maps
- a preliminary assessment of the role of spatial resolution on water and carbon simulated fluxes
- the methodology and first simulations of the use of HRLC product on a climate service of drought monitoring

Future versions of the Climate Assessment Report will incorporate analyses based on CRDP version 2 (including the contribution to Global Carbon Budget from deforestation maps), which is anticipated to be released midway through the project timeline. These updates will provide a comparative evaluation of the new data package and track its advancements over the previous version, ensuring a progressive improvement in addressing the scientific and practical challenges of climate research.

1.2 Purpose and scope

In this document, we report the methods/tools that we have developed to prepare the assessment of the HRLC products for climate modelling and the results obtained by the end of the first year of the project, based on the Phase 1 products. The overall strategy of the CRG for the HRLC products assessment is gathered into a single work package split into three case studies led by our three climate teams (LSCE, CREAM and UNEXE). Our main objectives are the following:

- Study the role of spatial resolution and vegetation type uncertainties on water and carbon fluxes and stocks.
- Study the contribution of the HRLC products in the time span integrated drought model which is the base of a drought climate service.
- Evaluation of the fractions of each 10m LC class at MR grid (300 m) on the cross-walking table (CWT) and the translation into ORCHIDEE PFTs.

	Ref	D5.1 - CAR		
	Issue	Date	Page	
	1.0	20/12/2024	3	

1.3 Applicable documents

Ref	Document ID	Document Title	Issue/Revision	Date
AD1		CCI HR Technical Proposal	v1.1	12/07/2023

1.4 Reference documents

Ref	Document ID	Document Title	Issue/Revision	Date

1.5 Acronyms and abbreviations



CHELSEA	Climatologies at high resolution for the Earth's land surface
CRU-JRA	Climatic Research Unit - Japanese Reanalysis
CWT	Cross Walking Table
ERA	European Reanalysis Anthropogenic and natural systems
HR	High Resolution
LC	Land Cover
MR	Medium Resolution
PFT	Plant Functional Type
SPEI	Standardized Precipitation Evapotranspiration Index
SPI	Standardized Precipitation Index

2 Role of spatial resolution and vegetation type uncertainties on the simulation of biogeochemical fluxes

The first case study is led by the LSCE team with the support of CREAM and the participation of UNIEXE. It is focused on two research axes [HRLC-TR-30]:

- study of the role of the spatial resolution on the simulation of the biogeochemical fluxes (and C and water stocks) with the ORCHIDEE land surface model.
- study of the role of the uncertainty of vegetation type on these same fluxes and stocks with ORCHIDEE and JULES models.

The first axis has been studied during the first year of the project based on first phase HRLC products and our preliminary results are presented in the following. We recall that the intercomparison with the JULES model will be done with the next HRLC products and, therefore, has not started.

	Ref	D5.1 - CAR		
	Issue	Date	Page	
	1.0	20/12/2024	4	

2.1 Role of spatial resolution on ORCHIDEE simulated biogeochemical fluxes

The investigation into the influence of spatial resolution on the simulation of biogeochemical fluxes, as well as carbon and water stocks, is being conducted using the ORCHIDEE land surface model. This analysis begins with the Phase 1 High-Resolution Land Cover (HRLC) products developed for three key static regions: Amazonia, Siberia, and Africa. The study utilizes land cover maps at varying spatial resolutions, ranging from 10 meters to 300 m. These maps are generated by aggregating the dominant vegetation types identified in the 10 m resolution land cover maps, ensuring consistency and accuracy across scales. By systematically comparing simulations across these resolutions, the study aims to uncover how spatial detail influences the accuracy and dynamics of biogeochemical flux predictions, including carbon uptake, water cycle processes, and overall ecosystem functioning.

2.2 Methodology

For the purposes mentioned in section 2.1, we worked with Phase 1 existing HRLC products on the three static regions (Amazonia, Siberia and Africa). The study of the role of the spatial resolution at 30m and 300m a was carried out on a different approach at 30 and 300m.

At 30m, we did this analysis in terms of HRLC classes and in terms of ORCHIDEE PFTs. Using the 10m High-Resolution Land Cover (HRLC) products as a base, resolution changes (raster pixel size) from 10 meters to 30 meters were implemented while maintaining the original alignment of the raster grid. This ensures consistency in spatial referencing and prevents shifts in the raster structure during rescaling.

The algorithm employed for this resolution adjustment is a contraction process designed specifically for categorical raster data. It operates by considering all values within the 30 m window and obtaining the **mode value**, representing the most frequently occurring category within the specified 30m aggregation window. In cases where there are multiple modal values (i.e., when two or more categories occur with equal frequency within the window), an impartial selection criterion is applied. This ensures that no particular category is favoured arbitrarily, maintaining objectivity in the aggregation process. The selected candidate in such scenarios is determined by a consistent and unbiased algorithmic approach, providing reproducibility and reliability in the resulting raster dataset (Masó et al. 2020).

This resolution change methodology is critical for maintaining the integrity and usability of the HRLC products when downscaling to coarser resolutions. It ensures that aggregated data remain representative of the underlying land cover distributions, making it suitable for applications such as land surface modelling, climate impact assessments, and large-scale ecological studies.

This scaling process was performed with the mosaic product for Sahel and Amazonia and at the tile level for the Siberia region, with each individual tile being independently resampled from 10 meters to 30 meters. The mosaic HRLC product is provided in longitude/latitude WGS84 (EPSG:4326). This reference system can introduce significant alterations in the number of pixels involved in the distorted grid for high latitudes (Snyder 1997). Thus, we used the HRLC product distributed in tiles at UTM for the corresponding zone (EPSG:32641, EPSG:32642, EPSG:32643, EPSG:32644, EPSG:32645, EPSG:32646) in the Siberia region. Following the completion of the resolution change for all tiles within a given region, the tiles were mosaicked into their corresponding UTM zone. Finally, the six UTM mosaics were transformed to EPSG:4326 and mosaicked again in one entire piece, to produce a seamless, continuous raster dataset for the entire region, ready for the ORCHIDEE comparison simulations., and the Land Cover maps at 30 m. The 300m was different, we compared these maps only in terms of ORCHIDEE PFTs. The idea was also to compare to a 300 m resolution such as the resolution of the MRLC maps. Because it does not make sense to aggregate the HRLC maps to a 300 m resolution with the same aggregation rule (dominant LC type) given that the legend is not adapted to such low resolution, we decided to make the comparison at the PFT level, in order to have a same comprehensive legend, allowing by this way to review our Cross Walking Table (CWT) translating the MRLC classes into generic PFTs.

In a second step, the ORCHIDEE PFT maps generated from the 10 m, 30 m and 300 m (MRLC) products have been used as boundary conditions of the ORCHIDEE model, to perform different simulations using the same atmospheric conditions and model implementations as in Phase 1 (CRU-JRA forcings). We present in this report

a preliminary analysis of the 10m and 30m PFT-based ORCHIDEE simulations. The aggregated products were computed by the CREAM team and the PFT analysis and ORCHIDEE simulations by the LSCE team.

2.3 Generation of fraction LC maps at 0.1° from 10m and 30m HRLC maps

The primary goal of this activity is to compare the ORCHIDEE simulations based on the current PFTs with those derived from a more spatially detailed approach. This approach uses fractions of each LC class at a High Resolution of 10m, aggregated with the MR grid (300m). These new PFTs will be evaluated and compared against the cross-walking table derived from Harper et al product (Harper et al 2023). New ORCHIDEE simulations at 0.125°, based on these updated PFTs will then be compared with existing simulations derived from MRLC Harpers' product.

The spatial relationship between the 300m pixel size and 10m pixel size is not homogeneous in latitude/longitude maps. Even in central latitudes, the calculation of LC classes fractions can be affected by this inconsistency. To address this issue, the HRLC UTM tiles product is used for fractions calculations, ensuring that the computations are performed within the corresponding UTM zones. This approach minimizes area distortions and improves the accuracy of the LC class fractions. Figure 2.1 illustrates the reprojected MR grid in the UTM system and the 10 m pixels of HRLC and the percent of the four existing classes in this zoom area, located around (-60° 50' 54.32", -15° 21' 4.40): tree cover evergreen broadleaf, tree cover deciduous broadleaf, shrub cover evergreen and grasslands.

In regard the fractions of static map 2019 into 300m grid, this document describes first results in the Amazonia region. The next CAR version will consolidate the completed results for the three project regions.

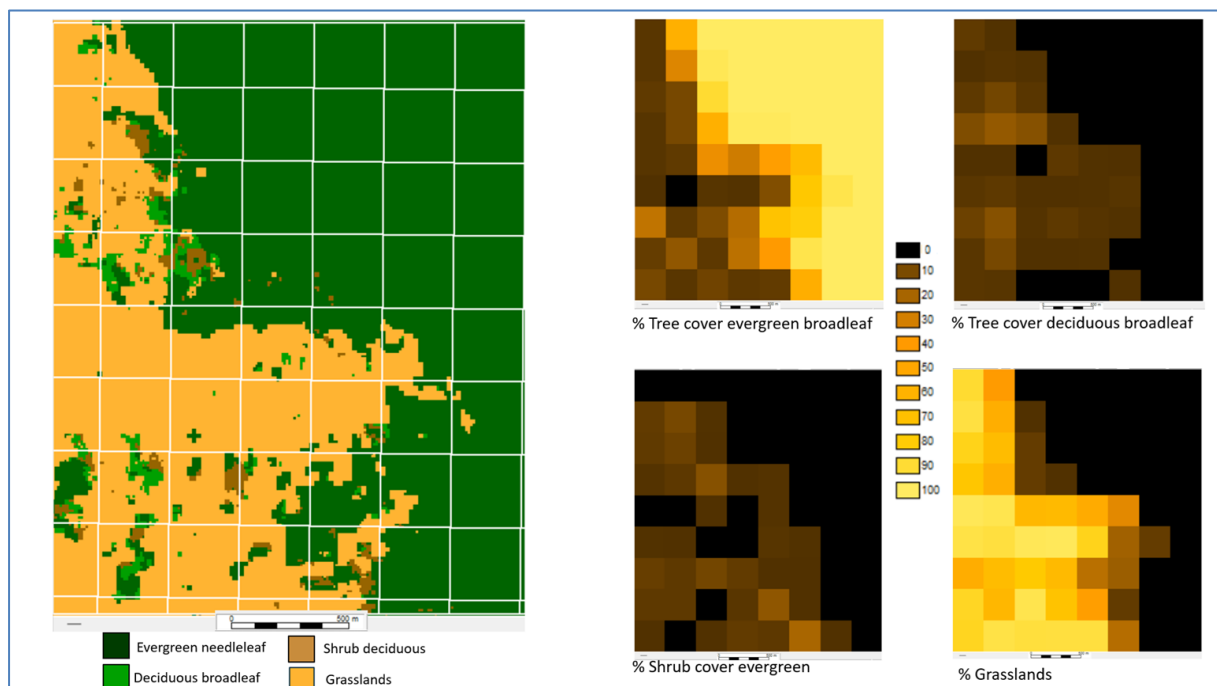


Figure 2.1: Zoom at local scale about the fractions for a 10m within 300m MR grid (white) map over Amazonia. On the left, HRLC map from UTM tiles; on the right, the four fraction maps (in %) product (lat/lon) of the 4 existing classes in this example region.

Two PFT datasets were generated at a spatial resolution of 0.1° using the HRLC static maps at 10m and 30m scales for 2019. To achieve this, the 10 m and 30 m HRLC maps were aggregated to compute the relative cover (ranging from 0 to 1) of each HRLC land cover class within coarser 0.1° grid cells (see Figure 2.2 for the Amazonia

region). These fractional land cover classes were then translated into ORCHIDEE-PFT maps through the integration of auxiliary data products.

The impact of spatial resolution on water, carbon, and energy fluxes was assessed using regional simulations with the ORCHIDEE land surface model. The simulations used the two PFT distribution maps derived from both the 10m and 30m HRLC datasets. The analysis focused on quantifying how differences in spatial resolution—through variations in PFT distributions—affect a set of climate-relevant variables. ORCHIDEE simulations were driven by ERA5-Land hourly atmospheric data (Muñoz-Sabater, 2019) for the 1999–2019 period, with PFT distribution maps corresponding to 2019 over the three static regions: Amazonia, Sahel, and Siberia.

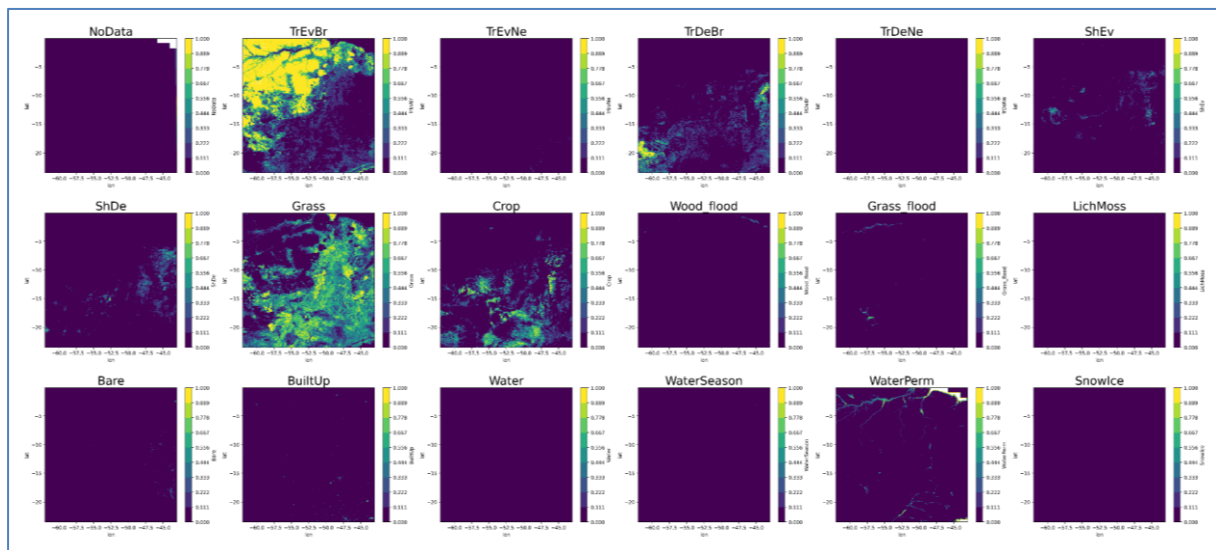


Figure 2.2: Fraction of HRLC classes at 0.1° from 10m HRLC map over Amazonia.

2.4 Comparison between 10m and 30m maps

Understanding the differences between PFT distributions (i.e. land cover fractions) derived from HRLC maps at 10m and 30m spatial resolutions is critical for assessing their implications on the subsequent ORCHIDEE modelling application. This section evaluates the consistency and variability between the fractional land cover datasets generated from the two resolutions, focusing on the impact of scale on land cover representation. By comparing the fractions obtained at 0.1° from 10m and 30m resolutions, we aim to identify spatial patterns, quantify discrepancies, and assess their influence on downstream processes, particularly the generation of PFT maps for environmental modelling. To better highlight the differences between PFT distributions derived from 10m and 30m HRLC maps, the 15 PFT categories were regrouped into five main categories: soil, deciduous trees (TrDe), evergreen trees (TrEv), grass and crops, as shown in Figure 2.3 for the Amazonia region. The PFT classes and their differences for each of the regions are described below.

2.4.1 over Amazonia

The dominant PFT class in this region is TrEv (evergreen broadleaf forests), particularly in the north-western part, which is the most homogeneous zone and almost entirely covered by the tropical evergreen PFT (see Figure 2.3). In contrast, the south-eastern part of the Amazonia region is more heterogeneous, with grasses being predominant and crops also occupying significant areas. It is important to note that water bodies, such as those in the Amazonian riverbeds, are classified as bare soils in the ORCHIDEE PFT scheme.

Figure 2.4 highlights the differences between PFT fractions derived from 30m and 10m HRLC maps (calculated as 30m PFT minus 10m PFT). Overall, the largest positive differences in PFT fractions occur where the corresponding PFT class is dominant. An exception to this is observed in the north-western part, where the TrEv

fraction is (almost) 1, resulting in negligible differences between the two resolutions due to the homogeneity of the area. For instance, the largest differences in soil PFT are located along the riverbeds, where the heterogeneity among water bodies, grasses and trees contributes to discrepancies. Differences in TrDe are prominent in two main patches in the southwestern and eastern parts of the region, aligning with areas where these TrDe classes are dominant. For grasslands, the differences are more widely distributed, following the spatial patterns of the grassland PFT. These differences are particularly pronounced in areas where grassland fractions are dominant but sufficiently heterogeneous, with values ranging between 0.55 and 0.85. In such cases, the coarser 30m HRLC maps tend to overestimate grassland fractions relative to the finer 10m resolution data. This analysis highlights how spatial resolution influences PFT distribution, particularly in heterogeneous regions such as south-eastern Amazonia, where land cover classes are more fragmented and mixed.

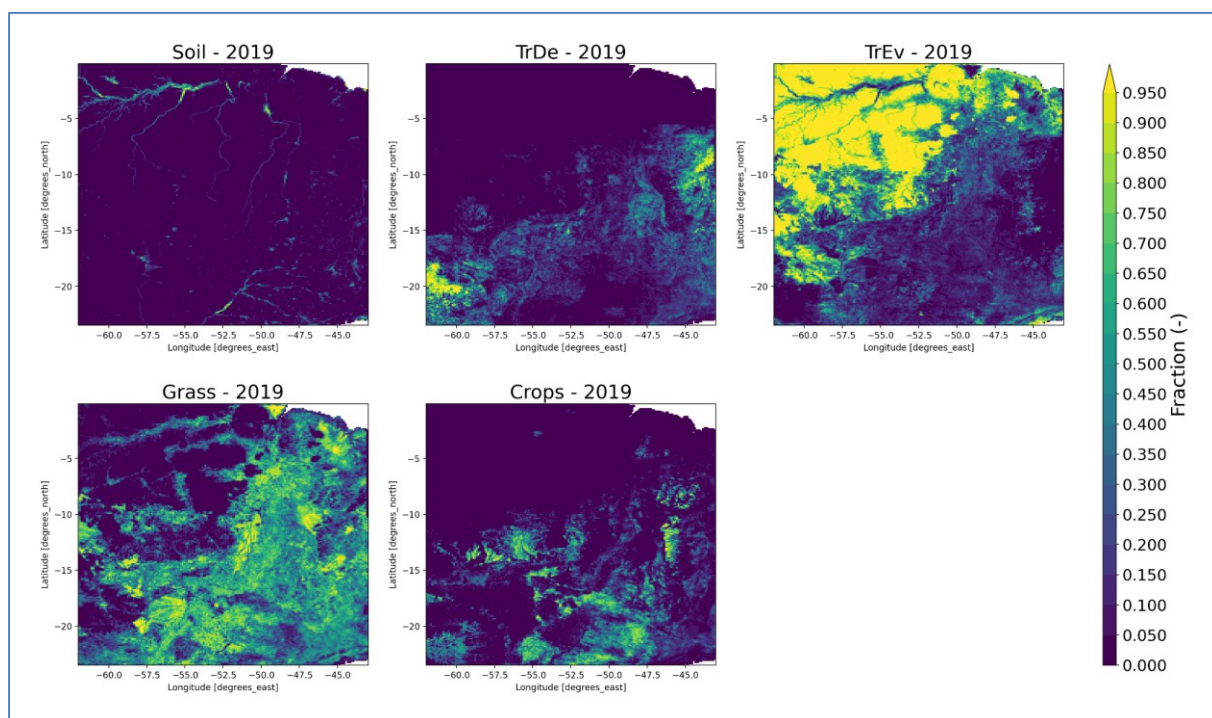


Figure 2.3: ORCHIDEE-PFTs maps built with 10m HRLC over Amazonia grouped into 5 main classes: soil, deciduous trees-TrDe, evergreen trees-TrEv, grass and crops.

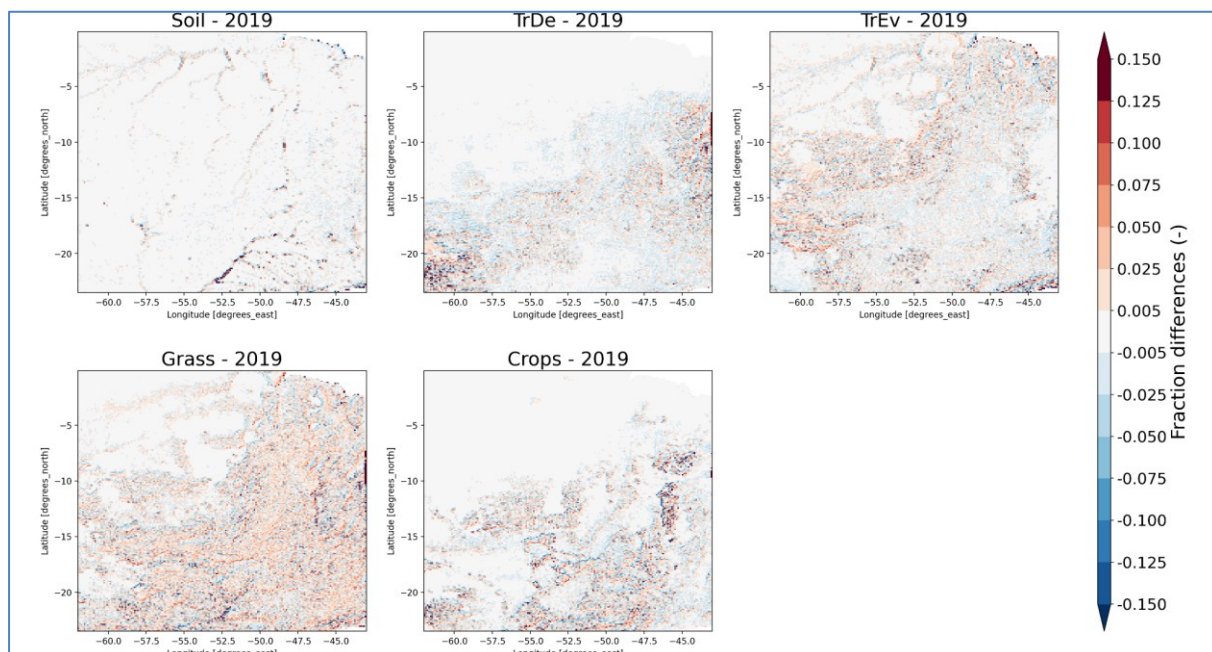


Figure 2.4: The PFT maps comparison between ORCHIDEE-PFTs from 30m HRLC and 10m HRLC over Amazonia grouped in 5 main classes: soil, deciduous trees-TrDe, evergreen trees-TrEv, grass and crops.

2.4.2 over the Sahel

Figure 2.5 illustrates the distribution of PFT classes across the Sahel region, highlighting a clear north-to-south gradient in vegetation types. In the northern part, bare soil dominates the landscape, reflecting the arid, desert conditions. Moving southward, deciduous trees (TrDe) become increasingly prominent in the transitional zone, while the more southern areas are characterized by the dominance of TrEv corresponding to dense tropical forests. Grasslands are widely distributed across the semiarid regions, extending from the southern edge of the desert to the northern boundary of the tropical evergreen forests. Grasslands are widely distributed across the semiarid regions, extending from the southern edge of the desert to the northern boundary of the tropical evergreen forests.

As observed in the Amazonia region, the largest positive differences in PFT fractions occur in areas where the corresponding PFT class is dominant but remains sufficiently heterogeneous (see Figure 2.6). In contrast, no significant differences are found in homogeneous areas, such as the bare soils of the desert in the north or the dense tropical evergreen forests in the south, where PFT fractions are close to 1. The most substantial differences are observed in the central part of the Sahel, where grasslands and TrDe are the primary vegetation types. These regions exhibit greater heterogeneity, leading to discrepancies between the 10m and 30m HRLC-derived PFT fractions. This highlights the sensitivity of PFT representation to spatial resolution in transitional and semiarid zones, where vegetation cover is more fragmented and mixed.

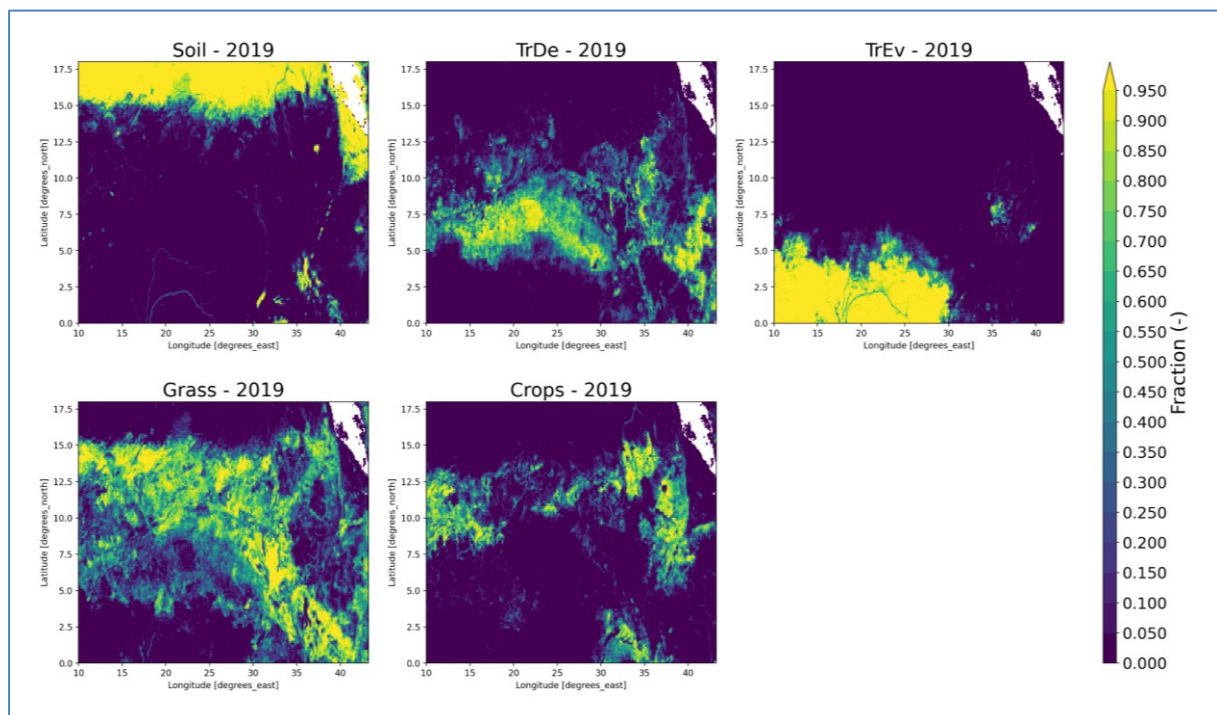


Figure 2.5: ORCHIDEE-PFTs maps built with 10m HRLC over the Sahel grouped into 5 main classes: soil, deciduous trees-TrDe, evergreen trees-TrEv, grass and crops.

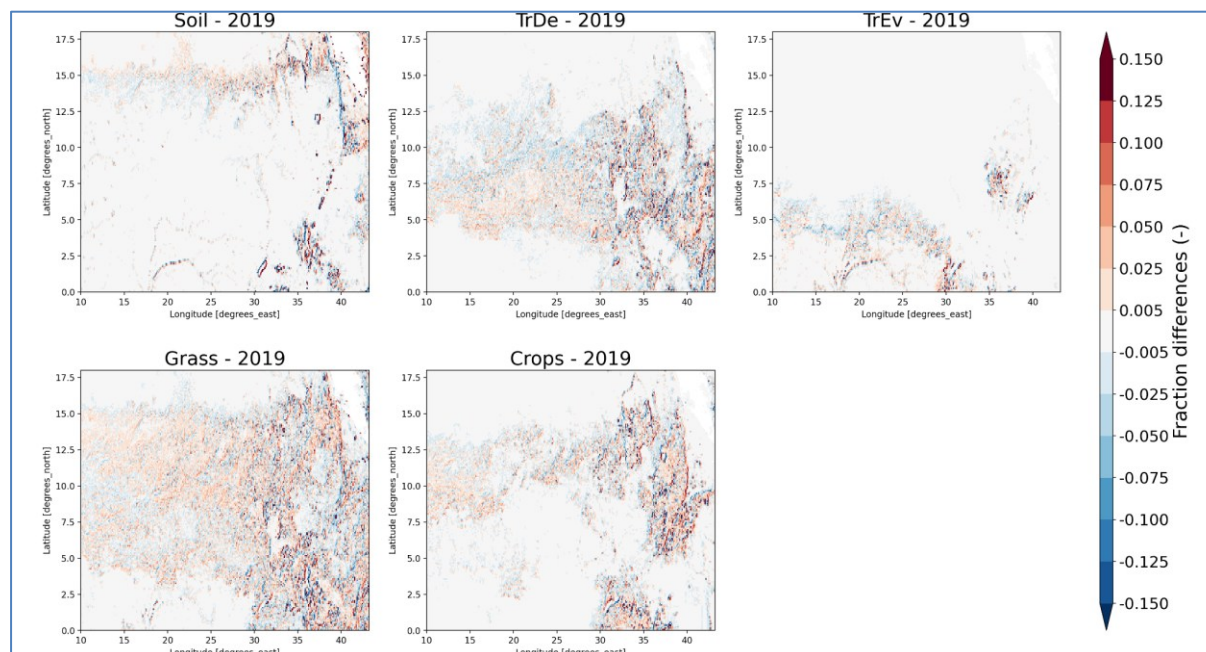


Figure 2.6: The PFT maps comparison between ORCHIDEE-PFTs from 30m HRLC and 10m HRLC over the Sahel grouped into 5 main classes: soil, deciduous trees-TrDe, evergreen trees-TrEv, grass and crops.

2.4.3 over Siberia

Figure 2.7 illustrates the distribution of PFT classes across the Siberia region, which, unlike Amazonia and Sahel, lacks large homogeneous areas where PFT fractions are close to 1. Grasslands are the most dominant PFT in Siberia, however, they are highly heterogeneous, with no extended continuous grassland areas. Soils PFT are widely dispersed across the region, primarily due to the presence of numerous scattered water bodies. The crop classes are concentrated in the south, which is the warmer part of the region, while the central part of the Siberia region is characterized by a mix of deciduous (TrDe) and evergreen trees (TrEv).

Figure 2.8 highlights the differences in PFT fractions across the Siberia region between the 10m and 30m HRLC-derived maps. In the northern areas, the largest positive differences are observed in grasslands, accompanied by negative differences in other PFT classes. This pattern reflects the heterogeneity of land cover in the northern regions, where fragmented vegetation and soil patches dominate. In the southern part of Siberia, the differences primarily occur between grasslands and crops, emphasizing the variability introduced by agricultural land use and the finer-scale fragmentation of vegetation. Overall, the Siberia region showcases the impact of spatial resolution in highly heterogeneous landscapes, where mixed vegetation, water bodies, and land cover transitions create significant differences in PFT fractions between 10m and 30m maps. Some artifacts linked to the different workflow in the mosaic product in the use of a more accurate geometric process are visible on the maps. The differences have been identified, CREA revised their processing, using a more similar mosaic workflow than the project product, and provided new maps which couldn't be included in this analysis due to lack of time.

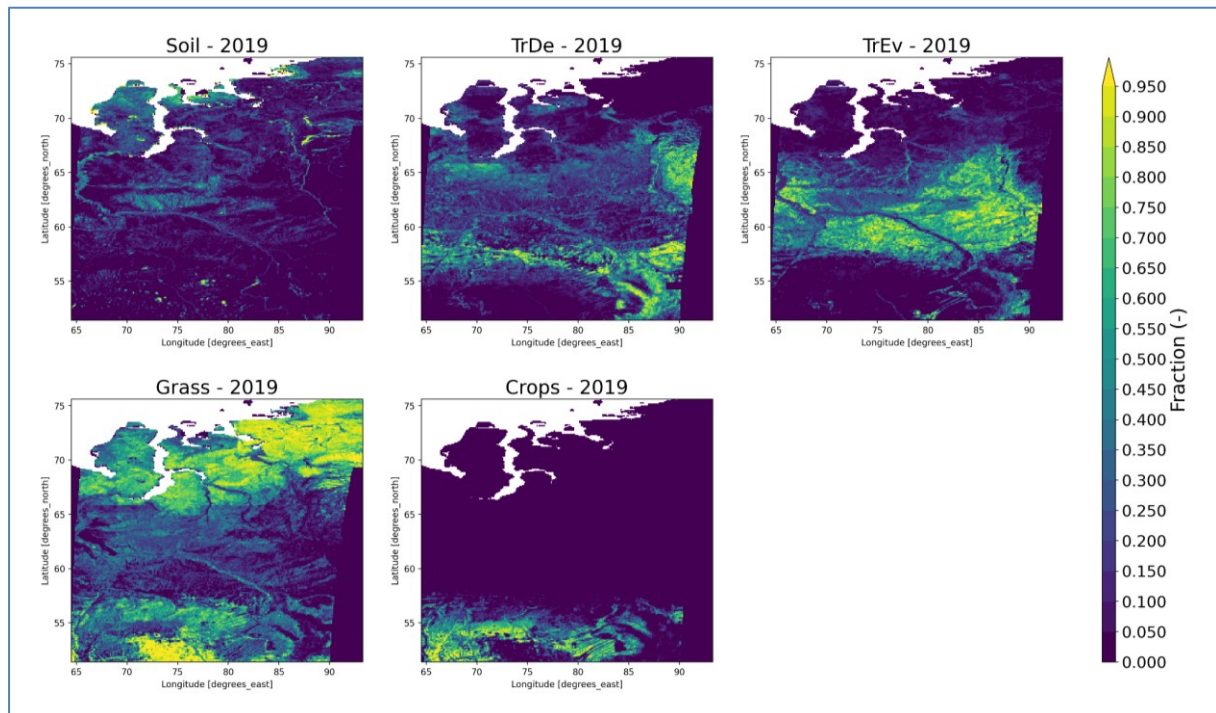


Figure 2.7: ORCHIDEE-PFTs maps built with 10m HRLC over Siberia grouped into 5 main classes: soil, deciduous trees-TrDe, evergreen trees-TrEv, grass and crops.

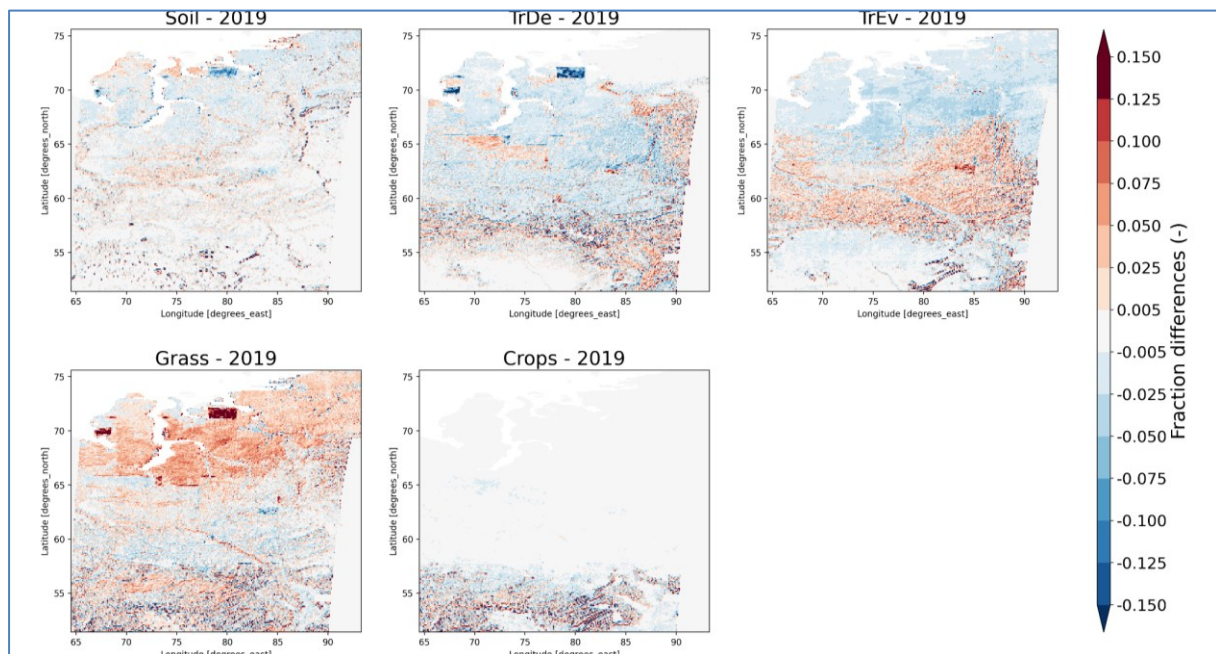




Figure 2.8: The PFT maps comparison between ORCHIDEE-PFTs from 30m HRLC and 10m HRLC over Siberia grouped into 5 main classes: soil, deciduous trees-TrDe, evergreen trees-TrEv, grass and crops.

2.5 Impacts on ORCHIDEE energy, water and carbon fluxes

In this section, we compare the results of two ORCHIDEE simulations performed, respectively, by applying the PFT maps at 0.1° from the 10m HRLC product (30m PFT) and the PFT maps at 0.1° derived from the 30m HRLC product (30m PFT). Both products are available for the three static regions in Amazonia, Sahel and Siberia for the year 2019.

	Ref	D5.1 - CAR		
	Issue	Date	Page	
	1.0	20/12/2024	11	

The analysis focuses on evaluating the impacts of the 10m PFT and 30m PFT maps on key energy, water, and carbon fluxes simulated by ORCHIDEE. Specifically, we assess changes in:

- Energy balance variables: surface albedo, land surface temperature, latent and sensible heat fluxes.
- Water balance variables: soil moisture, evaporation, transpiration, and interception.
- Carbon balance variables: gross primary production (GPP).

The results are presented as averaged differences between the two simulations (30m PFT minus 10m PFT) for the summer season. For the southern hemisphere (e.g., Amazonia), summer corresponds to December–January–February (DJF), while for the northern hemisphere (e.g., Sahel and Siberia), summer corresponds to June–July–August (JJA). This approach highlights the most significant changes in fluxes during the period of peak energy, water, and carbon exchanges. By examining these differences, we aim to quantify the sensitivity of ORCHIDEE-simulated fluxes to the spatial resolution of the PFT input maps and identify the key regions and variables most impacted by these differences. This analysis provides valuable insights into the role of spatial detail in land surface modelling and its implications for climate-relevant processes.

2.5.1. over Amazonia

Overall, the results indicate that the energy, water, and carbon fluxes are most significantly impacted in regions where differences between 30m PFT and 10m PFT are the largest. These larger differences occur in heterogeneous areas, whereas no differences are observed in homogeneous regions, where a single PFT fraction is close to 1 and consistently detected by both 10m and 30m HRLC products.

Figure 2.9 shows the ORCHIDEE simulations conducted using 10m PFT for the energy balance variables (top row in Figure 2.9) and the differences between using 30m PFT and 10m PFT maps (bottom row in Figure 2.9). For example, in the northeastern part of Amazonia, dominated by dense tropical forests, no significant differences are observed, as this region is spatially uniform and classified similarly by both PFT maps. In contrast, the rest of the region – characterized by more fragmented land cover – exhibits more notable impacts on fluxes. In the central part of Amazonia, latent heat flux shows negative differences (i.e., higher values simulated using 30m PFT). This can be attributed to an underestimation of deciduous trees (TrDe) and an overrepresentation of grasslands in 30m PFT relative to 10m PFT. In the western part of the region, both positive and negative differences are observed, particularly in surface albedo, land surface temperature, and sensible heat fluxes. These variations are driven by the heterogeneity of the landscape, where a mix of vegetation types – deciduous trees (TrDe), grasslands, and crops – forms a complex patchwork that is more accurately captured by the finer resolution of 10m PFT.

Figure 2.10 presents the ORCHIDEE simulations for water balance variables and GPP using 10m PFT (top row), alongside the differences between simulations using 30m PFT and 10m PFT (bottom row). Notable differences are observed in the Amazonian riverbeds, which stand out as heterogeneous ecosystems embedded within a homogeneous tropical forest where no significant differences occur. These differences in water balance variables highlight the impact of spatial heterogeneity, particularly in regions where water bodies (classified in soil PFT) are present. However, such differences are less apparent in the energy balance variables, as vegetated surfaces and water bodies in this region are not water-limited, reducing their sensitivity to spatial resolution changes. The largest and most widespread differences (relative to the absolute values of each variable) are found in interception loss, driven by the significant discrepancies in TrEv. This result underscores the critical role of evergreen forests in interception processes, where variations in PFT distributions between 10m PFT and 30m PFT maps lead to pronounced impacts on water balance simulations.

Overall, the results demonstrate that the spatial resolution of PFT input maps significantly influences ORCHIDEE-simulated fluxes in heterogeneous regions of Amazonia, particularly in areas where vegetation transitions and mixed land cover types dominate.

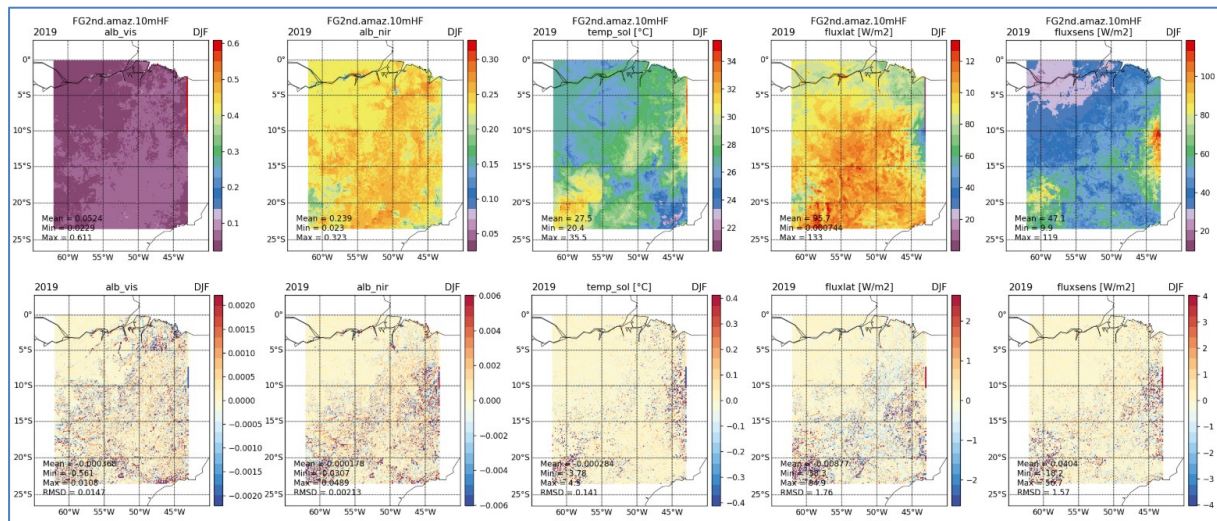


Figure 2.9: Energy budget variables modeled by ORCHIDEE using PFT maps built with HRLC at 10 m over Amazonia in summer months in the southern hemisphere (DJF) on the top. From left to right: visible albedo, near-infrared albedo, land surface temperature, latent heat flux and sensible heat flux. On the bottom, the simulation differences (30m PFT minus 10m PFT simulations) are plotted for the same period (DJF).

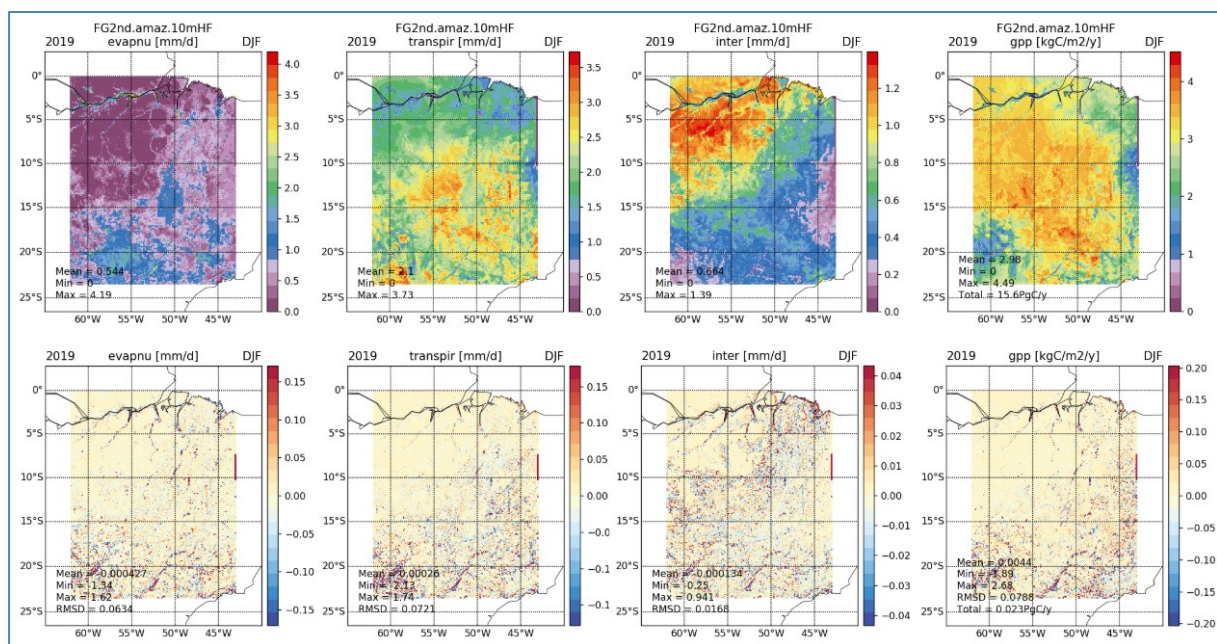


Figure 2.10: On the top from the left to right: soil evaporation, transpiration, interception loss and gross primary productivity modeled by ORCHIDEE using PFT maps built with HRLC at 10 m over Amazonia in summer months in the southern hemisphere (DJF). On the bottom, the simulation differences (30m PFT minus 10m PFT simulations) are plotted for the same period (DJF).

2.5.2 over the Sahel

Figures 2.11 and 2.12 present the ORCHIDEE simulations for energy, water and carbon variables using 10m PFT (top row) and the differences between simulations using 30m PFT and 10m PFT maps (bottom row). Consistent with the PFT distributions and their differences described in Section 2.4.2, a clear north-to-south gradient of vegetation is observed across the Sahel. This gradient is reflected in the energy, water and carbon variables, such as land surface temperature (Figure 2.11), where the hottest regions correspond to the arid desert areas in the north, and the coldest regions occur in the south, dominated by TrEv. In the same way, transpiration reflects well

this gradient from the absence of transpiration in the north and larger transpiration rates towards the south. As the northern and southern parts of the region are predominantly covered by a single PFT—bare soil in the north and TrEv in the south—no significant differences are observed in these areas for any energy, water and carbon flux. In contrast, the central part of the Sahel, transitioning from semiarid to more humid conditions, exhibits notable differences in fluxes. However, no clear spatial pattern emerges, reflecting the heterogeneous nature of this zone.

For latent heat flux, negative differences are observed in regions where deciduous trees (TrDe) are underrepresented and grasslands are overrepresented in the 30m PFT maps relative to 10m PFT. Moving further south, the opposite trend occurs, with grasslands being underrepresented in 30m PFT. The eastern part of the region is particularly heterogeneous, displaying larger differences in simulations without a clear spatial pattern, a characteristic typical of mixed land cover regions.

Overall, the central and eastern parts of the Sahel demonstrate the greatest sensitivity to differences in PFT spatial resolution, emphasizing the importance of fine-scale vegetation representation in regions with diverse and fragmented land cover.

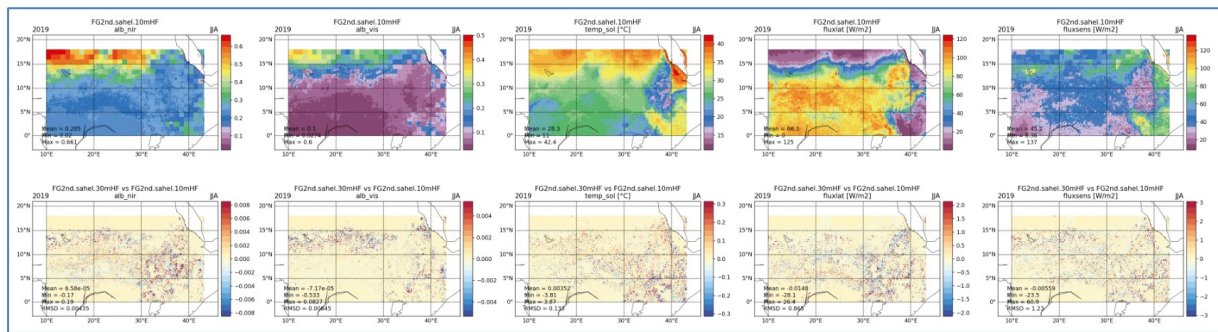


Figure 2.11: Energy budget variables modeled by ORCHIDEE using PFT maps built with HRLC at 10 m over the Sahel in summer months in the northern hemisphere (JJA) on the top. From left to right: visible albedo, near-infrared albedo, land surface temperature, latent heat flux and sensible heat flux. On the bottom, the simulation differences (30m PFT minus 10m PFT simulations) are plotted for the same period (JJA).

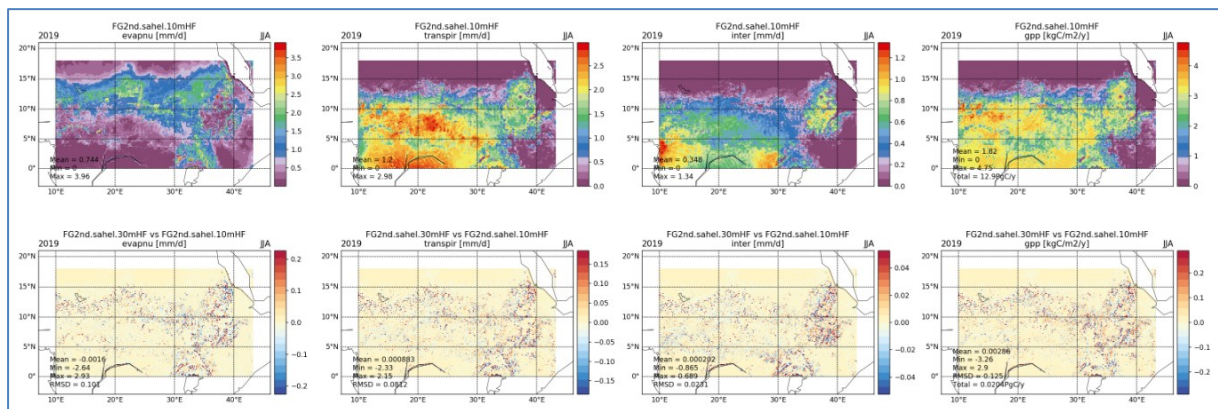




Figure 2.12: On the top from the left to right: soil evaporation, transpiration, interception loss and gross primary productivity modelled by ORCHIDEE using PFT maps built with HRLC at 10m over the Sahel in summer months in the northern hemisphere (JJA). On the bottom, the simulation differences (30m PFT minus 10m PFT simulations) are plotted for the same period (JJA).

2.5.3. over Siberia

The ORCHIDEE simulations over Siberia for energy, water, and carbon fluxes using 10m PFT and the differences between simulations using 30m PFT and 10m PFT maps are illustrated in Figure 2.13 and Figure 2.14. As highlighted in Section 2.4.3, Siberia exhibits the largest differences in PFT distributions, which lead to the most

	Ref	D5.1 - CAR		
	Issue	Date	Page	
	1.0	20/12/2024	14	

significant impacts on simulated energy, water, and carbon fluxes.

In northern Siberia, the 30m PFT map overrepresents grasslands at the expense of soil (including water bodies) and both deciduous (TrDe) and evergreen trees (TrEv). This overrepresentation of grasslands results in an overestimation of albedo (both visible and near-infrared), which in turn causes a reduction in land surface temperature and net radiation. Consequently, this reduces the turbulent fluxes – latent heat flux and sensible heat flux – in a proportional manner (Figure 2.13).

For water balance variables in northern Siberia, transpiration and interception loss remain largely unaffected by the differences in land cover, as the underrepresentation of trees (TrDe and TrEv) is compensated by the increase in grasslands under energy-limited conditions. However, soil evaporation decreases due to the underrepresentation of soil PFTs (including water bodies) in the 30m PFT map compared to the 10m PFT. In the central part of Siberia, negative differences in both deciduous trees and grasslands, combined with positive differences in evergreen trees, lead to notable impacts on water variables and carbon fluxes. Specifically, transpiration, interception loss, and GPP are overestimated in simulations using 30m PFT, reflecting the increased presence of evergreen trees in this region.

In southern Siberia, where grasslands and crops dominate, both positive and negative PFT differences are observed. This results in significant variability in the simulated fluxes without a clear spatial pattern, which is consistent with the behaviour observed in heterogeneous regions of Amazonia and Sahel.

It is important to note that some artifacts observed in the generation of the HRLC maps at both 10m and 30m resolutions persist in the ORCHIDEE simulations. Additionally, artifacts observed mainly in albedo, latent heat flux and soil evaporation can be attributed to the use of a coarse soil texture grid with a spatial resolution of 1° (compared to 0.1° of simulations), which introduces inconsistencies in the modelling of soil hydrological properties and processes. These issues will be addressed in future simulations by improving the generation of HRLC maps and employing a finer-resolution soil texture map to enhance the spatial representation of soil properties and reduce modelling artifacts.

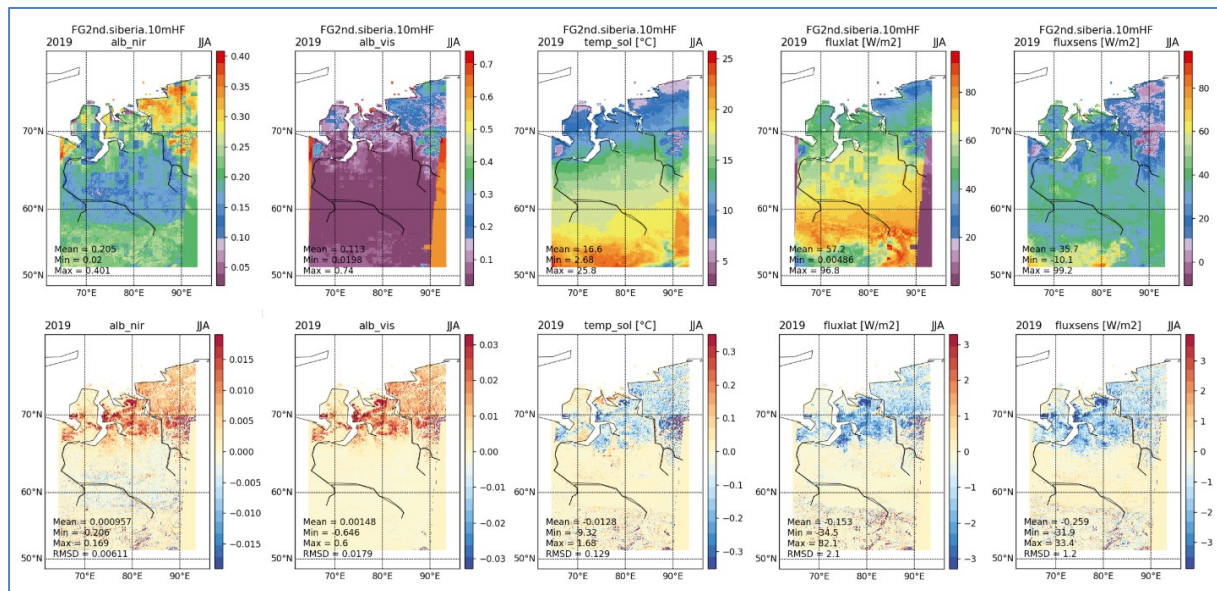


Figure 2.13: Energy budget variables modelled by ORCHIDEE using PFT maps built with HRLC at 10 m over Siberia in summer months in the northern hemisphere (JJA) on the top. From left to right: visible albedo, near-infrared albedo, land surface temperature, latent heat flux and sensible heat flux. On the bottom, the simulation differences (30m PFT minus 10m PFT simulations) are plotted for the same period (JJA).

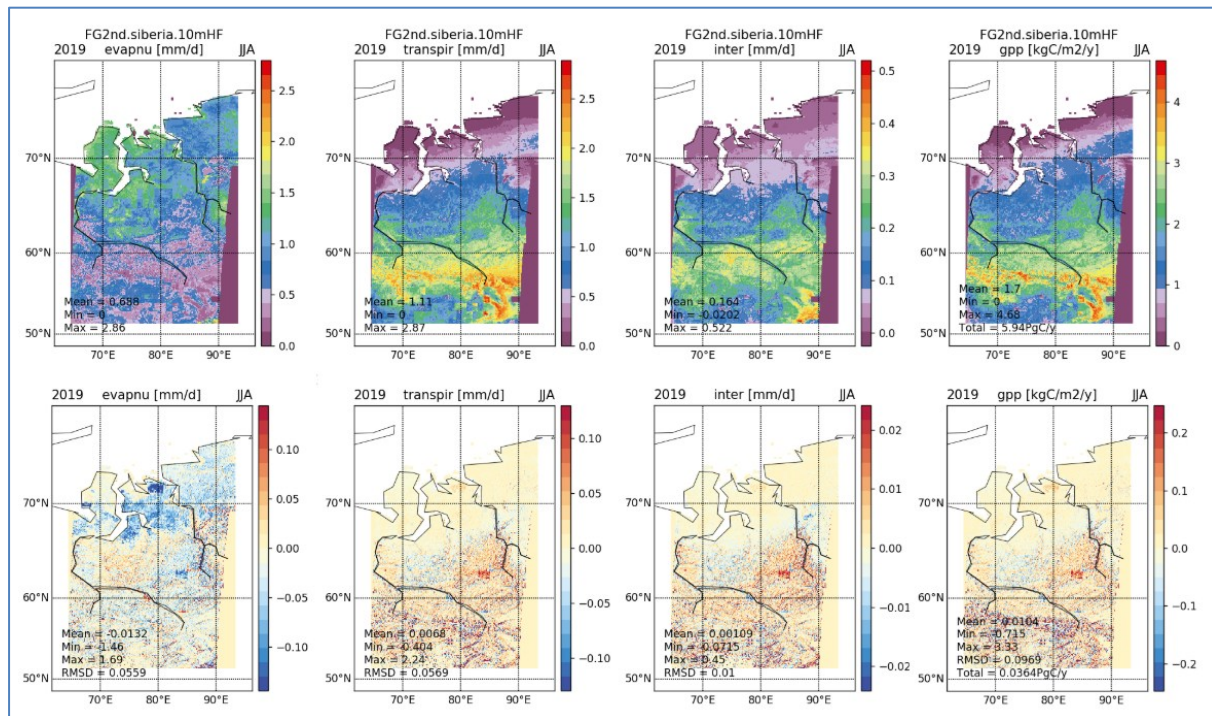


Figure 2.14: On the top from the left to right: soil evaporation, transpiration, interception loss and gross primary productivity modelled by ORCHIDEE using PFT maps built with HRLC at 10 m over Siberia in summer months in the northern hemisphere (JJA). On the bottom, the simulation differences (30m PFT minus 10m PFT simulations) are plotted for the same period (JJA).



3 Drought climate service

The second case study, conducted by CREAM, focuses on showcasing the added value and impact of incorporating Land Cover products, specifically HRLC, into a drought monitoring climate service. Traditionally, Land Cover has not been a key component in drought observatories. This study explores how including HRLC data may enhance the set of variables used in climate models, considering the importance of remote sensing products as key data sources for spatially regionalized climate modelling.

To demonstrate the added value and impact of incorporating Land Cover products, specifically HRLC, into a drought monitoring climate service, we will employ a Look-Up Table (LUT) approach. This LUT will serve as a tool to systematically identify which types of meteoroclimatic droughts have the most significant impacts on each land cover type. By associating specific drought metrics (e.g., drought indicators time spans) with distinct land cover categories, such as forests, grasslands, or croplands, the LUT will allow us to improve the accuracy of such climate services and to analyse the differential responses of various ecosystems to drought conditions. This approach not only highlights the critical role of high-resolution land cover data in refining climate service models but also provides a framework for targeted mitigation strategies based on land cover-specific vulnerabilities.

3.1 Climate data

Climate drought indicators, such as those based on the Standardized Precipitation Index (SPI), model the impacts of drought without explicitly accounting for land cover type. These models are often computed at various timescales depending on the specific drought impacts being monitored, such as agricultural, hydrological, or meteorological droughts. Since many of these models rely on precipitation and temperature as key inputs, the required data can be sourced from meteorological stations or existing climate models. In our case, we utilized the CHLSA database (Karger et al. 2017), which provides high-resolution climate data at 1 km spatial resolution from 1970 to 2018. This database was selected because its spatial coverage and temporal availability align most

	Ref	D5.1 - CAR		
	Issue	Date	Page	
	1.0	20/12/2024	16	

effectively with the objectives of our study, allowing us to achieve more accurate and comprehensive results.

Land cover types exhibit varying responses to drought, making it essential to tailor climate drought models by incorporating land cover-specific sensitivity factors. Integrating a land cover-based coefficient—such as those reflecting water retention capacity, evapotranspiration rates, or surface runoff—can enhance the accuracy of these models. This adjustment allows for a more nuanced representation of how different land cover types influence and are influenced by drought or wet conditions, ultimately improving the capacity of the models to reflect regional variations in drought impacts.

3.2 Look up table linking land cover types and drought models

An analysis of vegetation response to climate induced drought has been conducted to associate specific land cover types with tailored coefficients or time lags. Adjusting SPI (Standardized Precipitation Index) or SPEI time lags to different land cover types require careful consideration of water demands, vegetation characteristics, and resilience to drought. This highlights the critical importance of using high-resolution land cover maps, as they provide more detailed and accurate representations of land cover types, enabling the creation of more precise and reliable look-up tables (LUTs) for drought modelling.

1. **Tree cover evergreen broadleaf:** Long time lags (e.g., 12–24 months). These trees have a steady water requirement and are less responsive to short-term fluctuations.
2. **Tree cover evergreen needleleaf:** Medium to long time lags (e.g., 12 months). They tolerate drought better than broadleaf but require consistent water for growth.
3. **Tree cover deciduous broadleaf:** Medium time lags (e.g., 6–12 months). These trees shed leaves seasonally, making them more sensitive to shorter drought periods.
4. **Tree cover deciduous needleleaf:** Medium time lags (e.g., 6 months). Their seasonal growth cycles align with shorter precipitation changes.
5. **Shrub cover evergreen:** Medium time lags (e.g., 6–12 months). Evergreen shrubs are adapted to moderate drought and rely on consistent water availability.
6. **Shrub cover deciduous:** Short to medium time lags (e.g., 3–6 months). These shrubs respond quickly to precipitation changes due to their shallow roots.
7. **Grasslands:** Short time lags (e.g., 1–3 months). Grasslands are highly sensitive to short-term precipitation changes due to their fast-growing cycles.
8. **Croplands:** Short time lags (e.g., 1–3 months). Agricultural crops depend on immediate rainfall for productivity.
9. **Woody vegetation aquatic or regularly flooded:** Long time lags (e.g., 12–24 months). Flooded ecosystems rely on sustained precipitation and water retention.
10. **Grassland vegetation aquatic or regularly flooded:** Medium to long time lags (e.g., 6–12 months). These ecosystems depend on consistent moisture levels.
11. **Lichens and mosses:** Short time lags (e.g., 1–3 months). These organisms are highly responsive to immediate moisture availability.
12. **Bare areas:** No specific SPI lag, but short-term indicators (e.g., 1 month) can monitor soil moisture for potential revegetation.
13. **Built-up:** Not directly influenced by SPI but can consider short-term precipitation (e.g., 3-6 months) for urban water management.
14. **Open water seasonal:** Medium time lags (e.g., 3–6 months). Seasonal water bodies depend on timely precipitation.
15. **Open water permanent:** Long time lags (e.g., 12–24 months). Permanent water bodies rely on sustained hydrological inputs.

It is important to highlight that when using climate models incorporating temperature or evapotranspiration, these indicators are more sensitive to temperature fluctuations. As a result, they are particularly effective in capturing the water balance in region where temperature-driven evapotranspiration significantly impacts water availability. This approach is especially relevant for land covers sensitive to temperature variations, such as

grasslands, croplands and shrublands, where changes in temperature can have a pronounced impact on water dynamics.

1. **Grasslands and Croplands:** A slightly longer lag (e.g., 3–6 months) may be better for SPEI compared to SPI because evaporation impacts become evident after shorter precipitation deficits.
2. **Lichens, Mosses, and Bare Areas:** Evapotranspiration plays a minor role, so the lags remain the same as SPI (1–3 months).
3. **Woody Vegetation or Flooded Areas:** SPEI may require a more nuanced lag adjustment (e.g., 6–12 months for aquatic vegetation), as temperature impacts evaporation from water bodies.

SPEI is more responsive to **climate extremes**:

- For land cover types like **evergreen trees** and **permanent open water**, SPEI might require longer lags (12–24 months) in warm regions where rising temperatures amplify drought impacts.
- In temperate or cooler regions, SPI and SPEI lags would be similar because evapotranspiration's role is less pronounced.

Figure 3.1 summarizes the mentioned correspondences between HRLC classes and the time span drought indicators.






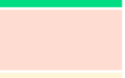









CLASS		SPI time lag	CLASS		SPI time lag
Tree cover evergreen broadleaf		12-24 months	Woody vegetation aquatic or regularly flooded		12-24 months
Tree cover evergreen needleleaf		9-12 months	Grassland vegetation aquatic or regularly flooded		9-12 months
Tree cover deciduous broadleaf		6-12 months	Lichens and mosses		1-3 months
Tree cover deciduous needleleaf		6-12 months	Bare areas		1 month
Shrub cover evergreen		6-12 months	Built-up		3-6 months
Shrub cover deciduous		3-6 months	Open water seasonal		6-12 months
Grasslands		1-3 months	Open water permanent		12-48 months
Croplands		1-3 months			

Figure 3.1: Table showing the correspondence between Land cover categories and climate drought indicators time lags.

3.3 Integration approach

The multidimensional nature of climate drought models—encompassing latitude, longitude, time, and time lags—can make their interpretation challenging for users. Incorporating land cover data not only enhances model accuracy but also provides a valuable means to simplify and integrate the time lag dimension. By consolidating the nine time spans typically involved into a single variable, the approach significantly reduces the volume of data while improving the usability and interpretability of the models for end-users.

The integration approach developed in this task begins with 12 monthly maps per year for each time lag (1, 3, 6, 9, 12, 18, 24, 36, and 48 months) of a selected climate drought model, such as SPI or SPEI. This results in over 100 climate drought model maps per year, all at a monthly resolution and 1 km spatial resolution. To enhance

the spatial and thematic accuracy, these maps will be integrated with high-resolution land cover maps at 30 m resolution. Fractions of each land cover category at the 30 m scale will be calculated for each 1 km pixel. These fractions will then be converted into coefficients, which will be applied to the climate drought model indicator values. The outcome will be a new, integrated, and synthesized climate drought model that combines the spatial precision of land cover data with the temporal detail of climate indicators.

This synthesized monthly map will (Figure 3.2) represent the maximum vulnerability impact of the climate drought model, taking into account the specific land cover types present within each 1 km climate pixel.

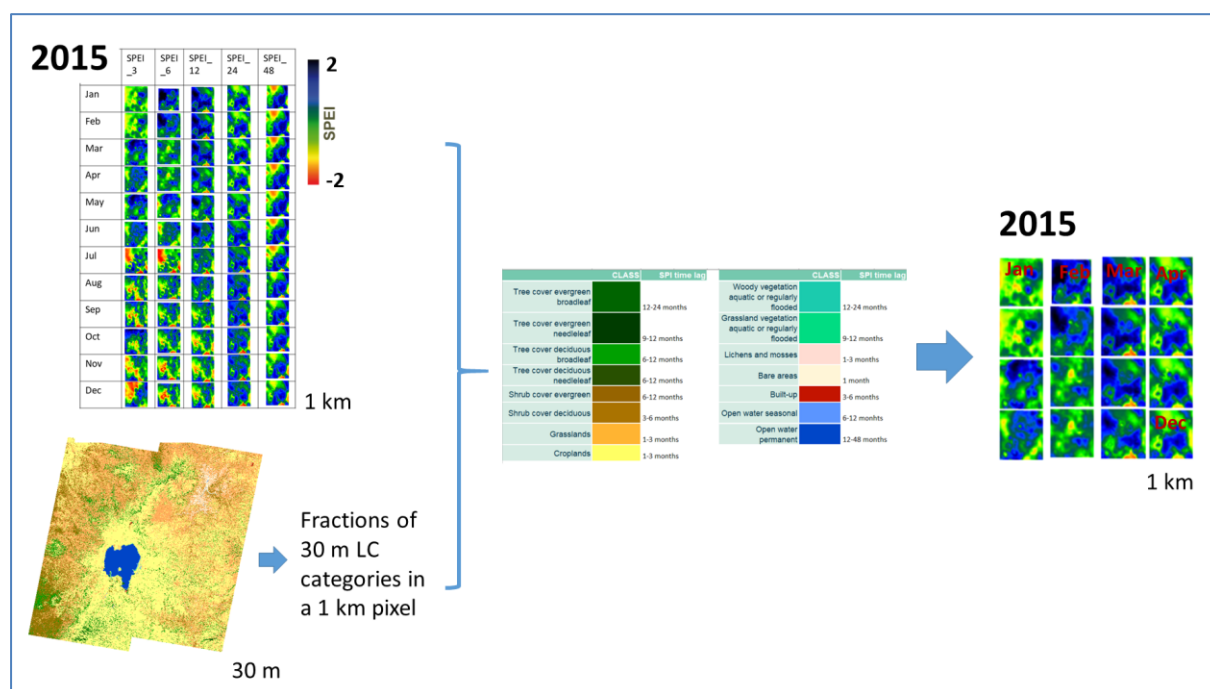


Figure 3.2: Integration approach scheme for Sahel region corresponding to tile h43 v15 of MR tiling system.

References



Karger, D.N., Conrad, O., Böhrner, J., Kawohl, T., Kreft, H., Soria-Auza, R.W., Zimmermann, N.E., Linder, P., Kessler, M. (2017): Climatologies at high resolution for the Earth land surface areas. *Scientific Data*. 4 170122. <https://doi.org/10.1038/sdata.2017.122>

Harper, K. L., Lamarche, C., Hartley, A., Peylin, P., Ottlé, C., Bastrikov, V., San Martín, R., Bohnenstengel, S. I., Kirches, G., Boettcher, M., Shevchuk, R., Brockmann, C., and Defourny, P. (2023) A 29-year time series of annual 300 m resolution plant-functional-type maps for climate models, *Earth Syst. Sci. Data*, 15, 1465–149 <https://doi.org/10.5194/essd-15-1465-2023> .

Masó, J.; Zabala, A.; Pons, X. (2020) Protected Areas from Space Map Browser with Fast Visualization and Analytical Operations on the Fly. Characterizing Statistical Uncertainties and Balancing Them with Visual Perception. *ISPRS Int. J. Geo-Inf.*, 9, 300. <https://doi.org/10.3390/ijgi9050300> .

Muñoz Sabater, J. (2019). ERA5-Land hourly data from 1981 to present, Copernicus Climate Change Service (C3S) Climate Data Store (CDS) <https://doi.org/10.5194/essd-13-4349-2021> .

Peng, L, Sheffield, J, Wei, Z, Ek, M, Wood, E.F. (2024) An enhanced Standardized Precipitation–Evapotranspiration

	Ref	D5.1 - CAR		
	Issue	Date	Page	
	1.0	20/12/2024	19	

Index (SPEI) drought-monitoring method integrating land surface characteristics. Volume 15, issue 5 ESD, 15, 1277–1300, <https://doi.org/10.5194/esd-15-1277-2024> .

Snyder J. P. (1997) *Map Projections, A Working Manual*, U.S. Geological Survey professional paper 1395.

Zhang, Y, Wang,P, Chen,Y, Yang, J, Wu, D, Ma, Y, Huo,Z, Liu,S. (2023) The optimal time-scale of Standardized Precipitation Index for early identifying summer maize drought in the Huang-Huai-Hai region, China. *Journal of Hydrology: Regional Studies*, Volume 46, 101350, ISSN 2214-5818, <https://doi.org/10.1016/j.ejrh.2023.101350>